Some perspectives about thermal Hall effects in correlated electron systems

Gang Chen
HKU

“Big picture”: thermal transports in Mott insulators

Low-T regime: proximate to ground state

Intermediate-T: correlated/cooperative paramagnet

High-T regime: trivial paramagnet

various q-particle description

T=0

T

反映基态和低能激发态性质

Transport of “un-particles”

may provide understanding about the interaction between local moments with **ETH**

[这里如果问我，我就解释我的crude理解]

There are some methods, but not conclusive at all.

Transports of magnon quasiparticles

Observation of the Magnon Hall Effect

Y. Onose,[1,2]* T. Ideue,[1] H. Katsura,[3] Y. Shiomi,[1,4] N. Nagaosa,[1,4] Y. Tokura[1,2,4]

Lu2V2O7

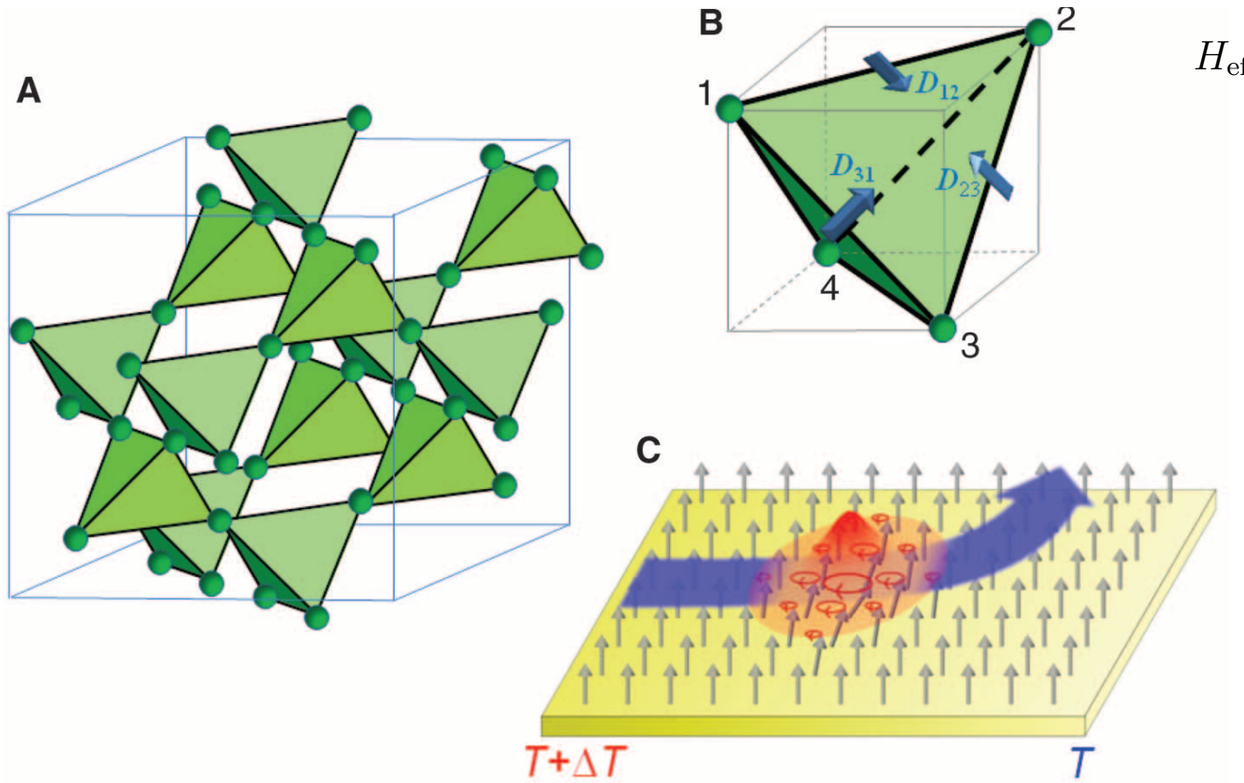

Fig. 1. The crystal structure of $Lu_2V_2O_7$ and the magnon Hall effect. (**A**) The *V* sublattice of $Lu_2V_2O_7$, which is composed of corner-sharing tetrahedra. (**B**) The direction of the Dzyaloshinskii-Moriya vector $\vec{D}_{ij}$ on each bond of the tetrahedron. The Dzyaloshinskii-Moriya interaction $\vec{D}_{ij} \cdot (\vec{S}_i \times \vec{S}_j)$ acts between the *i* and *j* sites. (**C**) The magnon Hall effect. A wave packet of magnon (a quantum of spin precession) moving from the hot to the cold side is deflected by the Dzyaloshinskii-Moriya interaction playing the role of a vector potential.

$$H_{\rm eff} = \sum_{\langle ij \rangle} -J\vec{S}_i \cdot \vec{S}_j + \vec{D}_{ij} \cdot (\vec{S}_i \times \vec{S}_j) - g\mu_{\rm B}\vec{H} \cdot \sum_i \vec{S}_i = \sum_{\langle ij \rangle} h_{ij},$$

$$\begin{aligned} h_{ij} &= -J\vec{S}_i \cdot \vec{S}_j + D^n_{ij}(S^l_i S^m_j - S^l_i S^m_j) - \frac{H}{6}(S^n_i + S^n_j) \\ &= -\frac{J}{2}(S^+_i S^-_j + S^-_i S^+_j) - JS^n_i S^n_j + i\frac{D^n_{ij}}{2}(S^+_i S^-_j - S^-_i S^+_j) - \frac{H}{6}(S^n_i + S^n_j) \\ &= -\frac{J_{ij}}{2}(e^{-i\phi_{ij}} S^+_i S^-_j + e^{i\phi_{ij}} S^-_i S^+_j) - JS^n_i S^n_j - \frac{H}{6}(S^n_i + S^n_j), \end{aligned}$$

where $J_{ij} = \sqrt{J^2 + (D^n_{ij})^2}$ and $\tan\phi_{ij} = D^n_{ij}/J$.

$$S^n_i = S - b^\dagger_i b_i, \quad S^+_i = (2S - b^\dagger_i b_i)^{1/2} b_i, \quad S^-_i = b^\dagger_i (2S - b^\dagger_i b_i)^{1/2},$$

$$h_{ij} \sim -J_{ij}S(e^{-i\phi_{ij}} b^\dagger_i b_j + e^{i\phi_{ij}} b^\dagger_j b_i) + \left(JS + \frac{H}{6}\right)(b^\dagger_i b_i + b^\dagger_j b_j).$$

DMI works as vector gauge potential for magnons

Transports of magnon quasiparticles

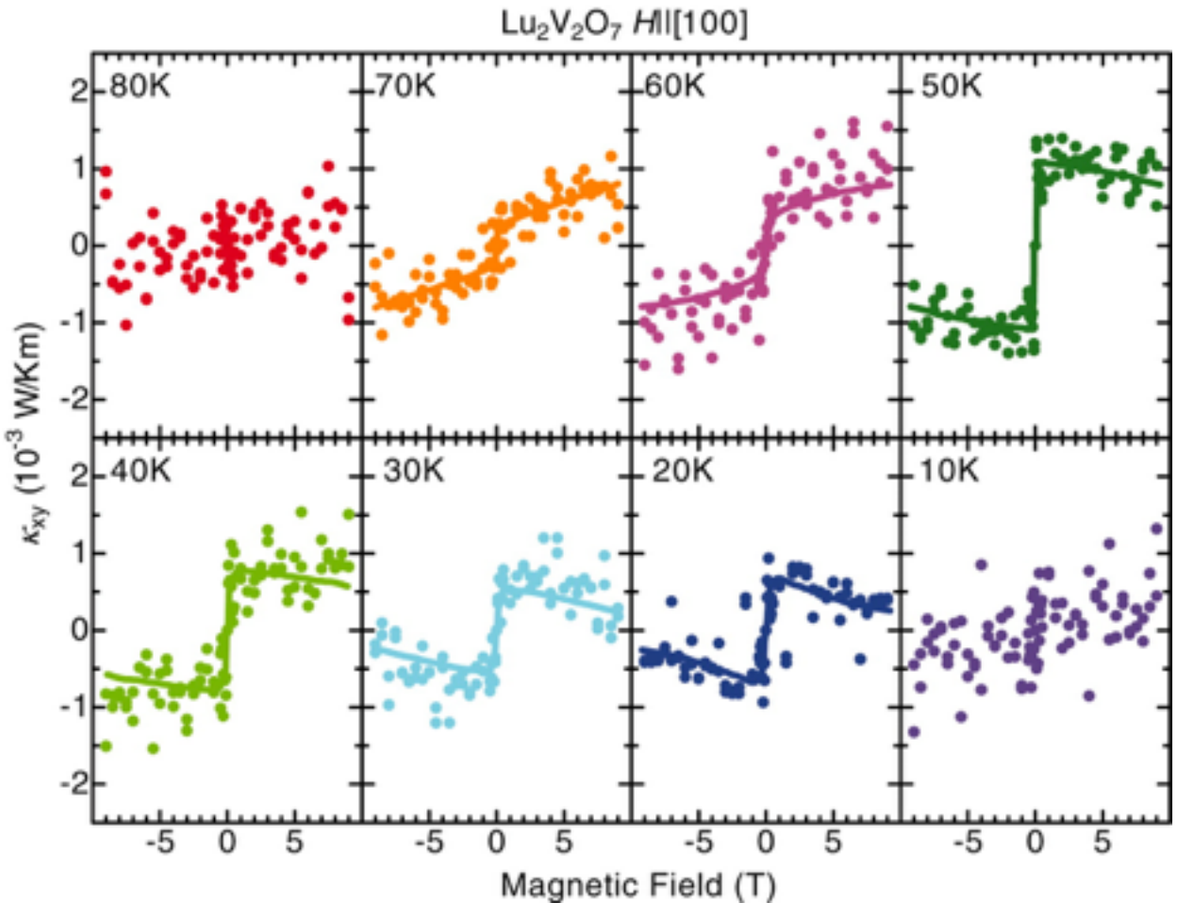

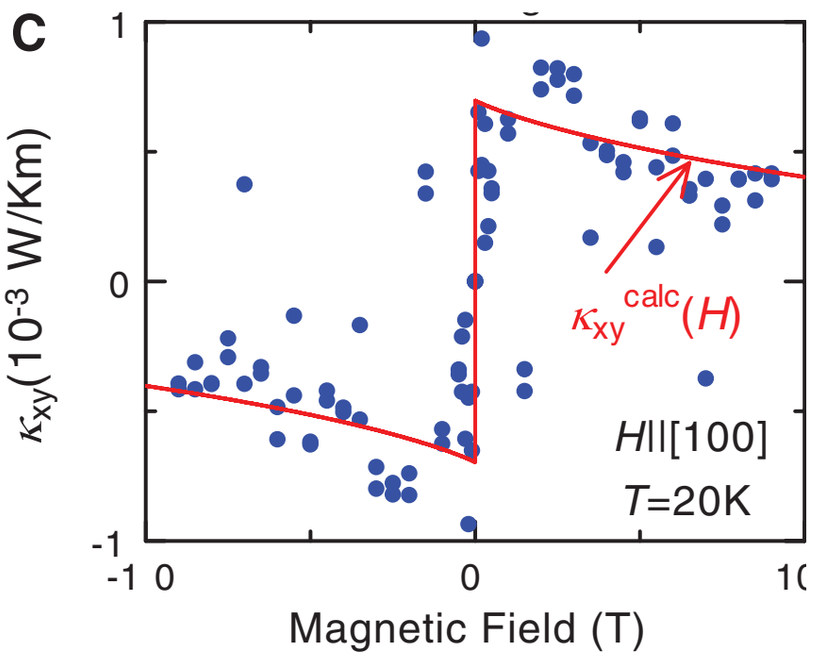

$$\kappa_{\alpha\beta} = -\frac{1}{2T}\mathrm{Im}\sum_{m=1}^{4}\int_{\mathrm{BZ}}\frac{d^3k}{(2\pi)^3}n_{\mathrm{B}}[\omega_m(\vec{k})]\left\langle\frac{\partial u_m(\vec{k})}{\partial k_\alpha}\middle|[H_{\mathrm{SW}}(\vec{k})+\omega_m(\vec{k})]^2\middle|\frac{\partial u_m(\vec{k})}{\partial k_\beta}\right\rangle,$$

1. transport is from thermally activated magnons
2. Thermal Hall is from magnon Berry curvature
3. kxy/T ->0 as T ->0 due to the magnon gap in many cases.

The semiclassical language is effective Lorentz force.

Giant thermal Hall conductivity in the pseudogap phase of cuprate superconductors

G. Grissonnanche[1]*, A. Legros[1,2], S. Badoux[1], E. Lefrançois[1], V. Zatko[1], M. Lizaire[1], F. Laliberté[1], A. Gourgout[1], J.-S. Zhou[3], S. Pyon[4,5], T. Takayama[4,6], H. Takagi[4,6,7,8], S. Ono[9], N. Doiron-Leyraud[1] & L. Taillefer[1,10]*

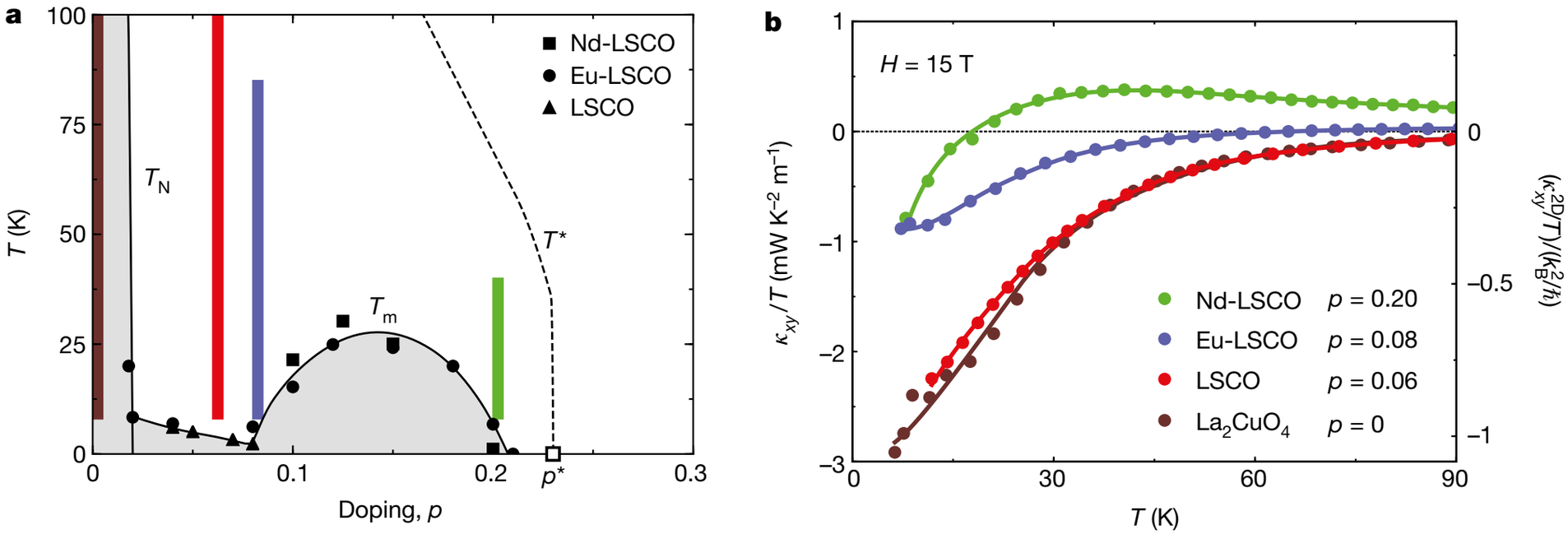

Fig. 1 | Phase diagram and thermal Hall conductivity of cuprates. **a**, Temperature–doping phase diagram of Nd-LSCO, Eu-LSCO and LSCO, showing the antiferromagnetic phase below the Néel temperature T_N and the pseudogap phase below T^* (ref. [29]), which ends at the critical doping $p^* = 0.23$ for both Nd-LSCO (ref. [17]) and Eu-LSCO (ref. [30]). For LSCO, $p^* \approx 0.18$ (ref. [29]). Short-range incommensurate spin order occurs below T_m, as measured by μSR on Nd-LSCO (squares[21]), Eu-LSCO (circles[31]) and LSCO (triangles[32]). The coloured vertical strips indicate the temperature range where the thermal Hall conductivity κ_{xy}/T at the corresponding doping decreases towards negative values at low temperature (see **b**). **b**, Thermal Hall conductivity κ_{xy}/T versus temperature in a field $H = 15$ T, for four materials and dopings as indicated, colour-coded with the vertical strips in **a**. On the right vertical axis, the magnitude of κ_{xy}/T is expressed in fundamental units of thermal conductance per plane ($k_B^2/\hbar$).

Violation of W-F law

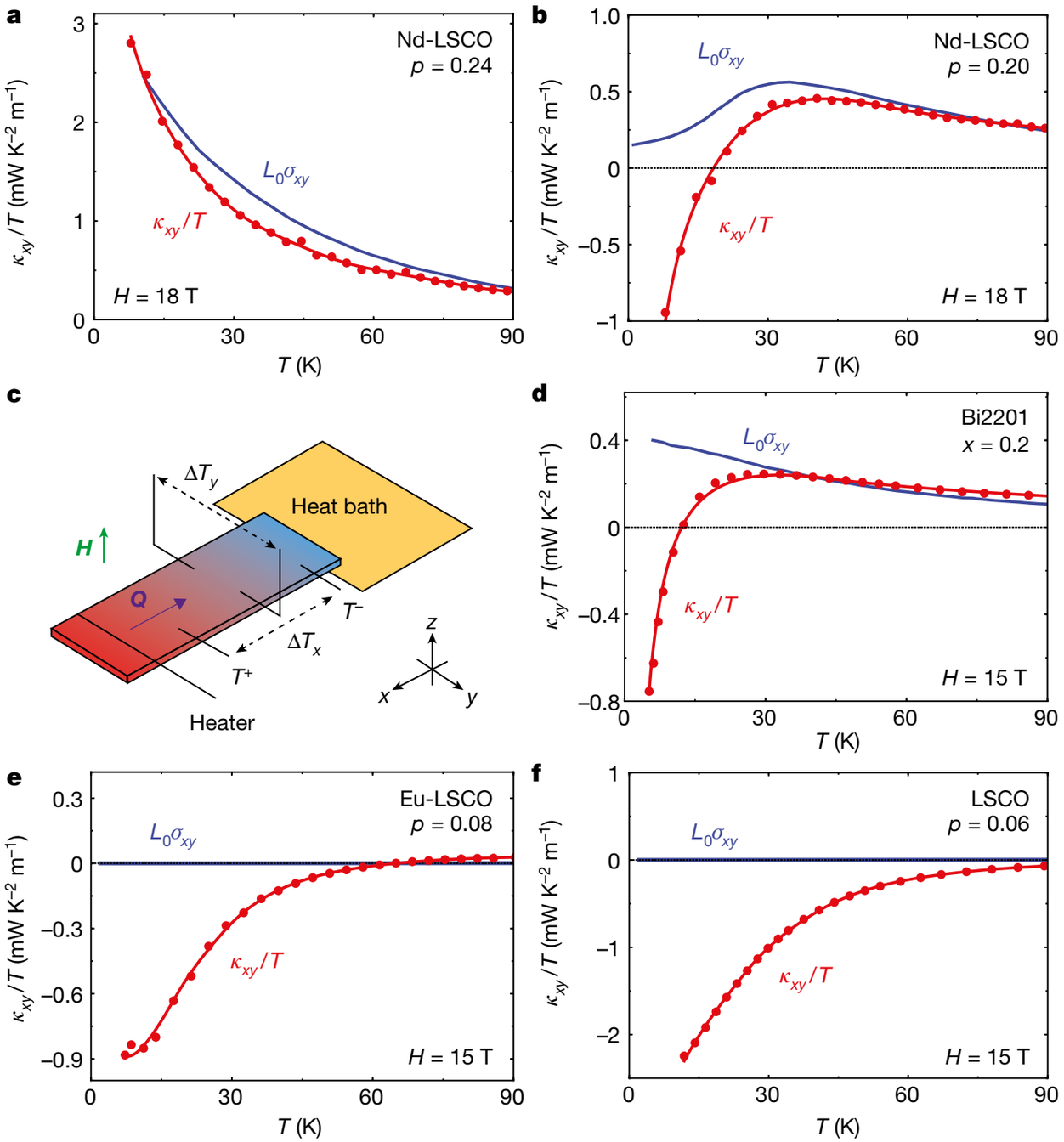

Fig. 2 | Thermal and electrical Hall conductivities of four cuprates. Data panels show thermal Hall conductivity κ_{xy}, plotted as κ_{xy}/T (red), and electrical Hall conductivity σ_{xy}, expressed as $L_0\sigma_{xy}$ (blue), where $L_0 = (\pi^2/3)(k_B/e)^2$, as a function of temperature: the material, its doping p and field H are indicated. **a**, **b**, Nd-LSCO; **c**, sketch of the thermal Hall measurement set-up (see Methods); **d**, Bi2201; **e**, Eu-LSCO; and **f**, LSCO.

(For Nd-LSCO $p = 0.20$ (**b**), σ_{xy} was measured[17] at $H = 33$ T.)
In Nd-LSCO at $p = 0.24$, κ_{xy}/T and $L_0\sigma_{xy}$ are both positive at all temperatures and they track each other, satisfying the Wiedemann–Franz law in the $T = 0$ limit. By contrast, for $p < p^*$ in all four materials, κ_{xy}/T falls to large and negative values at low temperature, whereas $L_0\sigma_{xy}$ remains positive.

Sign reversal across p*

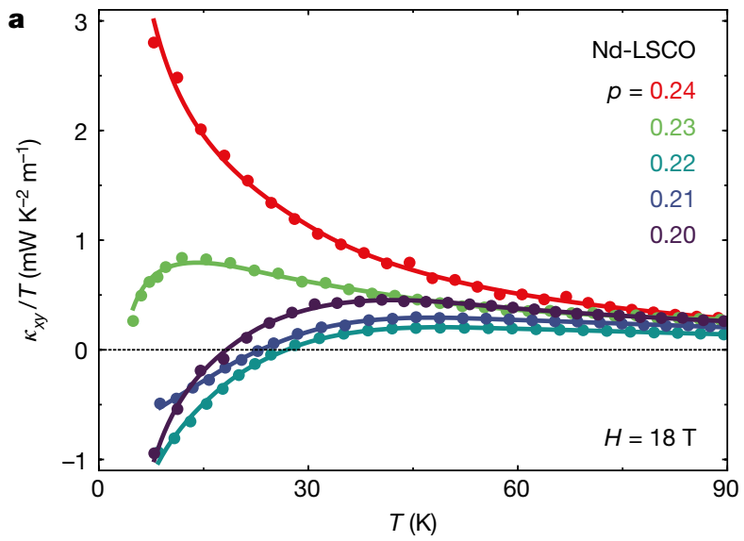

Fig. 3 | Thermal Hall conductivity across the pseudogap critical point *p.** Shown is thermal Hall conductivity κ_{xy}/T for Nd-LSCO in $H = 18$ T (**a**) and Eu-LSCO in $H = 15$ T (**b**), at dopings as indicated, on both sides of the pseudogap critical point $p^* = 0.23$. In both materials, κ_{xy} becomes negative at low temperature when $p < p^*$.

Linearly increase with field

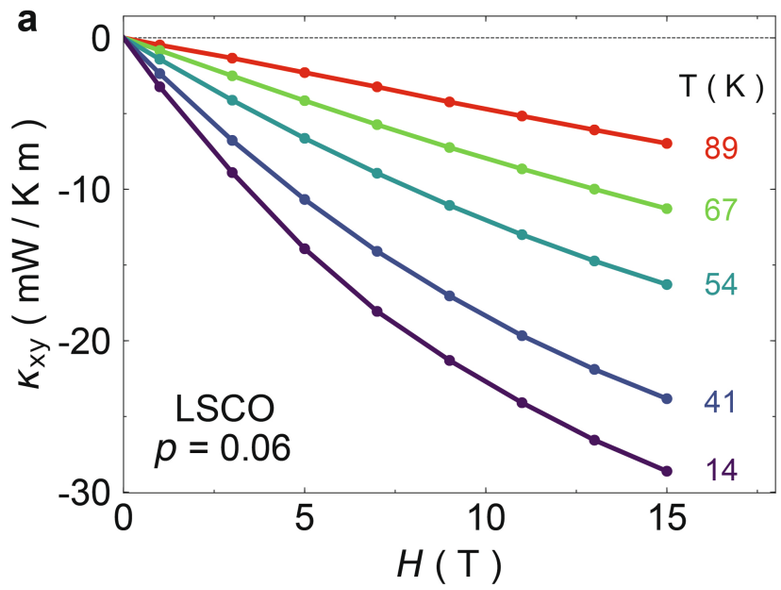

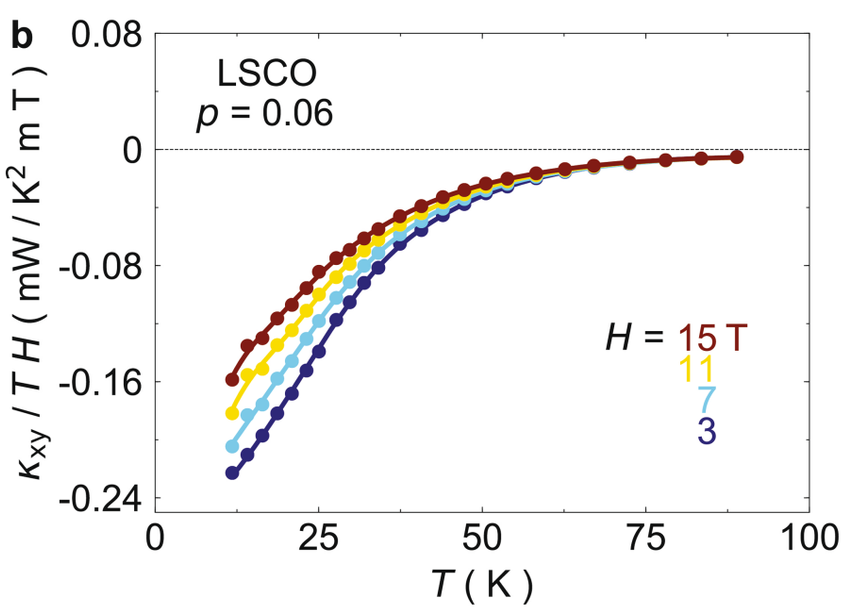

Extended Data Fig. 4 | Magnetic field dependence of κ_{xy} in LSCO. **a**, Field dependence of the thermal Hall conductivity of LSCO at $p = 0.06$, plotted as κ_{xy} versus H at various temperatures, as indicated (data points).

The dependence of κ_{xy} on H is linear at high T and it becomes sublinear at lower T. **b**, Deviation from linearity displayed by plotting $\kappa_{xy}/(TH)$ versus T at four different fields H, as indicated (data points).

Table 1 | Thermal Hall conductivity in various insulators

Material	κ_{xy} (mW K^{-1} m^{-1})	κ_{xx} (W K^{-1} m^{-1})	$\lvert\Delta\kappa_{xx}\rvert$ (W K^{-1} m^{-1})	$\lvert\Delta\kappa_{xx}/\kappa_{xx}\rvert$	T (K)	H (T)	Reference
La_2CuO_4	−38.6	12.4	~0.06	~0.005	20	15	This work
LSCO	−30.0	5.1	~0.02	~0.004	15	15	This work
Eu-LSCO	−13.2	4.5	~0.015	~0.003	15	15	This work
pyrochlore FM ← $Lu_2V_2O_7$	1.0	0.75	ND	ND	50	9	[28]
$Fe_2Mo_3O_8$	24	9	5	0.55	45	14	[3]
$(Fe,Zn)_2Mo_3O_8$	24	10	3.2	0.32	30	9	[3]
3d pyrochlore ice QSL ← $Tb_2Ti_2O_7$	1.2	0.37	0.12	0.32	15.5	8	[12]
2d Kitaev QSL ← $RuCl_3$	8	15.5	0.62	0.04	20	15	[4]
2d Kitaev QSL ← $RuCl_3$	3.5	8	0.45	0.055	35	16	[23]
2d kagome QSL ← Ca kapellasite	1.1	0.2	ND	ND	16	15	[6]
2d honeycomb or triangular QSL ← $Ba_3CuSb_2O_9$	0.008	0.07	0.0035	0.05	5	15	[20]

Maximal value of the thermal Hall conductivity κ_{xy} (second column) in various insulators (first column), compared to our three cuprates (the first three entries, namely, La_2CuO_4, LSCO $p = 0.06$ and Eu-LSCO $p = 0.08$), measured at temperature T and field H as indicated (columns 6 and 7 respectively): the ferromagnet $Lu_2V_2O_7$ (ref. [28]); the multiferroic ferrimagnets $Fe_2Mo_3O_8$ and $(Fe_{0.875}Zn_{0.125})_2Mo_3O_8$ (ref. [3]); the spin-ice material $Tb_2Ti_2O_7$ (ref. [12]); and the spin-liquid candidates $RuCl_3$ (refs [4,23]), Ca kapellasite[6] and $Ba_3CuSb_2O_9$ (ref. [20]). We also list the thermal conductivity κ_{xx} measured at the same temperature, in zero field (third column). The change induced in κ_{xx} by the field, $\Delta\kappa_{xx} = \kappa_{xx}(H) - \kappa_{xx}(0)$, is given in absolute and relative terms (fourth and fifth column, respectively). ND, not determined.

Puzzle of experiments

Most striking is **large** thermal Hall effect in the Mott insulating phase [with no doping].

Thermal Hall transport is from the charge neutral particles/excitations in the Mott phase.

Thermal Hall effect kxy/T is as large as a quantized one.

Help us to understand

What is really the “parent” Mott state of high-Tc SC ?

What is inside the soup of excitations in the underdoped regime?

Magnon does not work

Quote from **Consideration of Thermal Hall Effect in Undoped Cuprates**

Jung Hoon Han,[1,*] Jin-Hong Park,[1] and Patrick A. Lee[2,†]

on the whole is an attempt to fit the observation. On the experimental side, the renormalized spin-wave theory does a good job in accounting for the magnetic excitations in the square-lattice antiferromagnet, as revealed for instance in recent experiments [49, 50]. On the other hand, some high-energy features in the magnetic excitation are not fully explained within the spin-wave theory alone [49, 50], which in turn prompted speculations about residual spinon excitations in the Heisenberg model [51].

ior under the magnetic field. In the spin-wave scenario, a magnon gap inevitably opens and suppresses magnon contribution to transport. For the spinon-based scenario,

This paper was written in a very honest way.

The story of Subir's theory

1. The Mott insulator Neel state is proximate to Neel-VBS transition.

2. This DQCP is likely dual to Dirac fermions [recent theory development].

3. A sizable scalar spin chirality from magnetic field generates a Dirac mass and convert the system into a chiral spin liquid.

4. The field could drive a transition from Neel to Neel+CSL state.

Predictions: chiral edge states? surface sheath state?
Neel to Neel+CSL transition driven by magnetic field, this topological transition has some interesting properties.

?issues: 1. whether the system is proximate to Neel-VBS transition?
2. whether the field coupling to scalar spin chirality is large enough to take care of the experiments?

Enhanced thermal Hall effect in the square-lattice Néel state

Rhine Samajdar[1], Mathias S. Scheurer[1], Shubhayu Chatterjee[2], Haoyu Guo[1], Cenke Xu[3] and Subir Sachdev[1*]

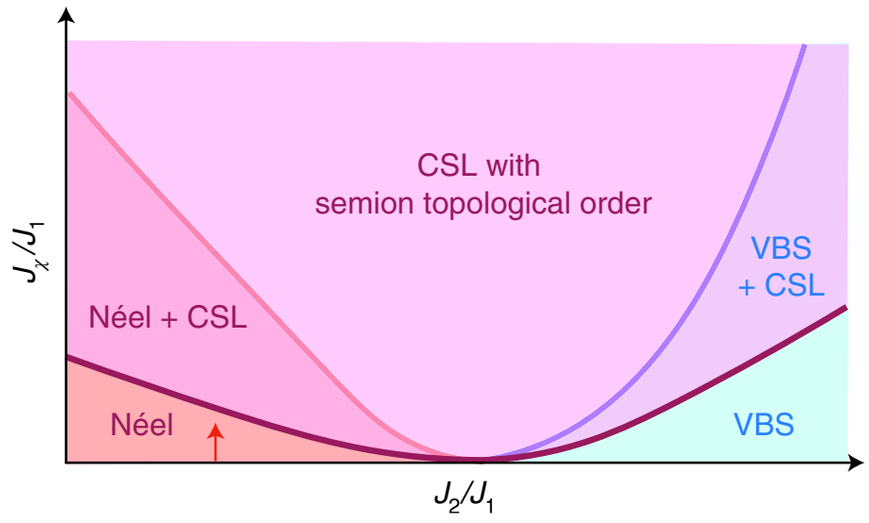

Fig. 1 | Schematic of proposed phase diagram of $H_1 + H_B$ at $B_Z = 0$. (See Fig. 3a for a phase diagram with non-zero $\mathbf{B}_Z$.) By varying the first, J_1, and second, J_2, nearest-neighbour exchange interactions and the orbital coupling J_χ in equation (2), the antiferromagnet on the square lattice shows phases with combinations of Néel, VBS and chiral spin liquid (CSL) topological order. The phase boundaries are presumed to meet at an SO(5)-symmetric (near) critical point at which J_χ is a relevant perturbatio and the phase boundaries all scale as $J_\chi \approx |J_2 - J_{2c}|^{\lambda_\chi/\lambda_2}$; we expect $\lambda_\chi/\lambda_2 > 1$. Here, we imagine starting from the Néel state at zero magnetic field ($J_\chi = 0$), close to the boundary of the VBS order such that a small value of field-induced J_χ can already drive the system close to the phase boundary with Néel + CSL (indicated by the red arrow). The existence of an SO(5) critical point is not a precondition for a continuous Néel to Néel + CSL transition.

We are interested in spin $S = 1/2$ antiferromagnets with spin operators $\mathbf{S}_i$ on the sites i of the square lattice and Hamiltonian $H = H_1 + H_B$. The first term has the form

$$H_1 = \sum_{i<j} J_{ij} \mathbf{S}_i \cdot \mathbf{S}_j + \ldots \tag{1}$$

$$H_B = J_\chi \sum_{\triangle} \mathbf{S}_i \cdot (\mathbf{S}_j \times \mathbf{S}_k) - \sum_i \mathbf{B}_Z \cdot \mathbf{S}_i \tag{2}$$

tesimal J_χ is a relevant perturbation. The phase diagram we propose for the square-lattice J_1–J_2–J_χ antiferromagnet is summarized in Fig. 1, and the critical spin liquid is realized by the deconfined critical point at $J_\chi = 0$ between the Néel and valence bond solid (VBS)

$$\mathcal{L}_{\mathrm{SO}(5)} = i\bar{\psi}_a \gamma^\mu (\partial_\mu - iA_\mu)\psi_a + m_\chi \bar{\psi}_a \psi_a \tag{8}$$

where $a = 1, 2$ is the flavour index.

The SO(5) symmetry is apparent after we express $\mathcal{L}_{\mathrm{SO}(5)}$ in terms of Majorana fermions. The fermion mass $m_\chi \propto J_\chi$ is also SO(5) invariant and is a perturbation on the putative SO(5)-invariant Néel–VBS critical point at $m_\chi = 0$. It is plausible that m_χ is a relevant perturbation on such a critical point (with scaling dimension $\lambda_\chi > 0$); then an infinitesimal J_χ will be sufficient to drive the critical antiferromagnet into the chiral spin liquid phase. If the Néel–VBS transition is weakly first-order, then a very small value of J_χ will be sufficient. Tuning away from

This proximity to Neel-VBS is independent from Neel-Neel+CSL.

Mean-field theory for Neel-Neel+CSL

Our analysis starts from a model[20] of the square-lattice Néel state as the confining phase of an SU(2) gauge theory of fluctuations about a 'π-flux' mean-field state[22]. In this formulation, the spins are represented by fermionic spinons $f_{i\alpha}$, via $\mathbf{S}_i = (1/2) f^{\dagger}_{i\alpha} \boldsymbol{\sigma}_{\alpha\beta} f_{i\beta}$, where

$$H_f = -\sum_{i<j} \left(t_{ij} f^{\dagger}_{i\alpha} f_{j\alpha} + t^{\star}_{ij} f^{\dagger}_{j\alpha} f_{i\alpha} \right)$$

$$-\tfrac{1}{2} \sum_i \left(\mathbf{B}_Z + \eta_i \mathbf{N} \right) \cdot f^{\dagger}_{i\alpha} \boldsymbol{\sigma}_{\alpha\beta} f_{i\beta}.$$

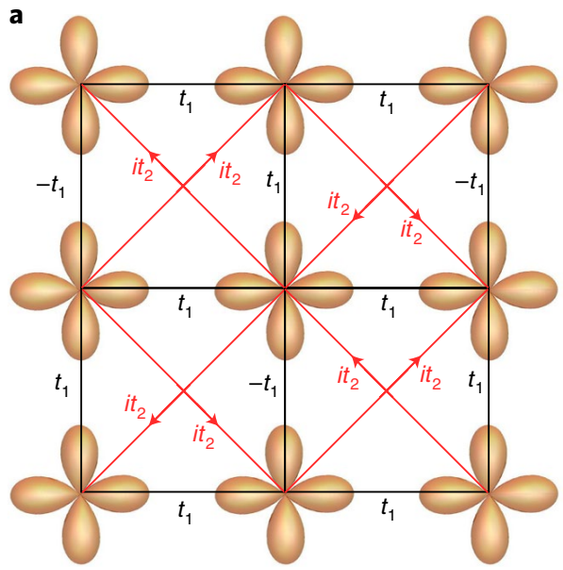

it2 takes care of U(1) gauge flux (scalar spin chirality),
Neel order is taken as a mean-field treatment.

$$\kappa_{xy} = -\frac{k_B^2}{\hbar T} \int d\varepsilon \, \varepsilon^2 \sigma_{xy}(\varepsilon) f'(\varepsilon) \qquad (4)$$

where $\sigma_{xy}(\varepsilon) = -\int_{\varepsilon_{n\mathbf{k}} < \varepsilon} d^2k \, \Omega_{n\mathbf{k}} / (4\pi^2)$ is $\hbar/e^2$ times the Hall conductivity, and $f(\varepsilon)$ is the Fermi distribution function at energy ε. The corresponding Chern number is

$$C_n = \frac{1}{2\pi} \int d^2k \, \Omega_{n\mathbf{k}} \in \mathbb{Z} \qquad (5)$$

As T approaches 0,

$$\frac{\kappa_{xy}}{T} = -\frac{\pi k_B^2}{6\hbar} \sum_{n \in \text{filled bands}} C_n \qquad (6)$$

correction from Chern-Simon term

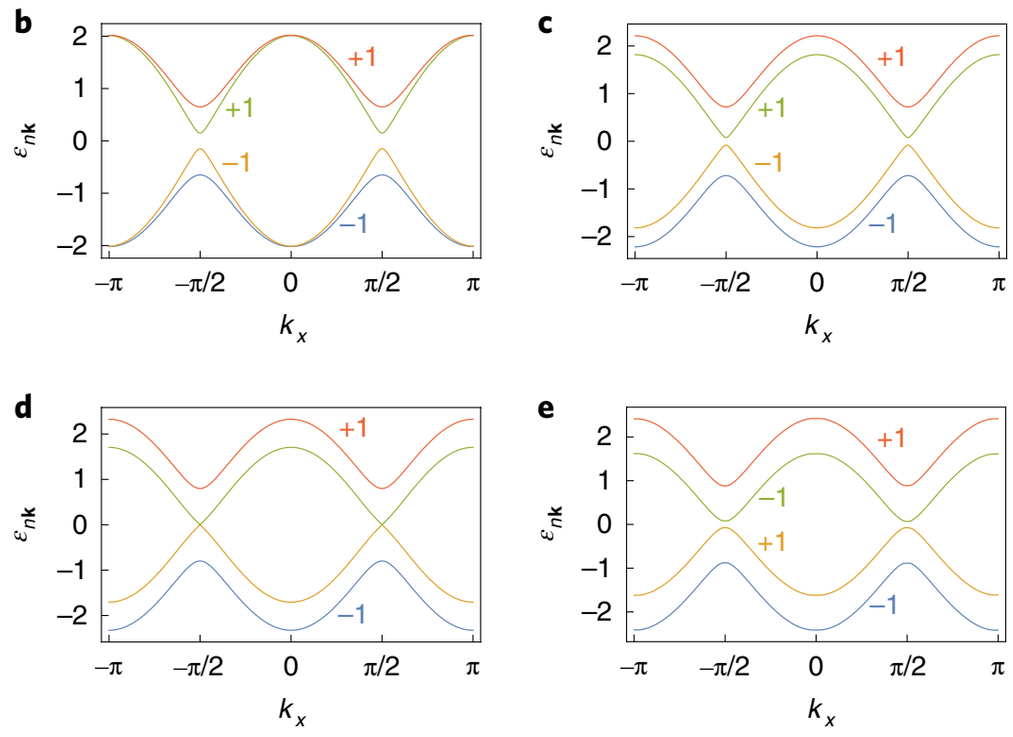

Neel-Neel+CSL transition

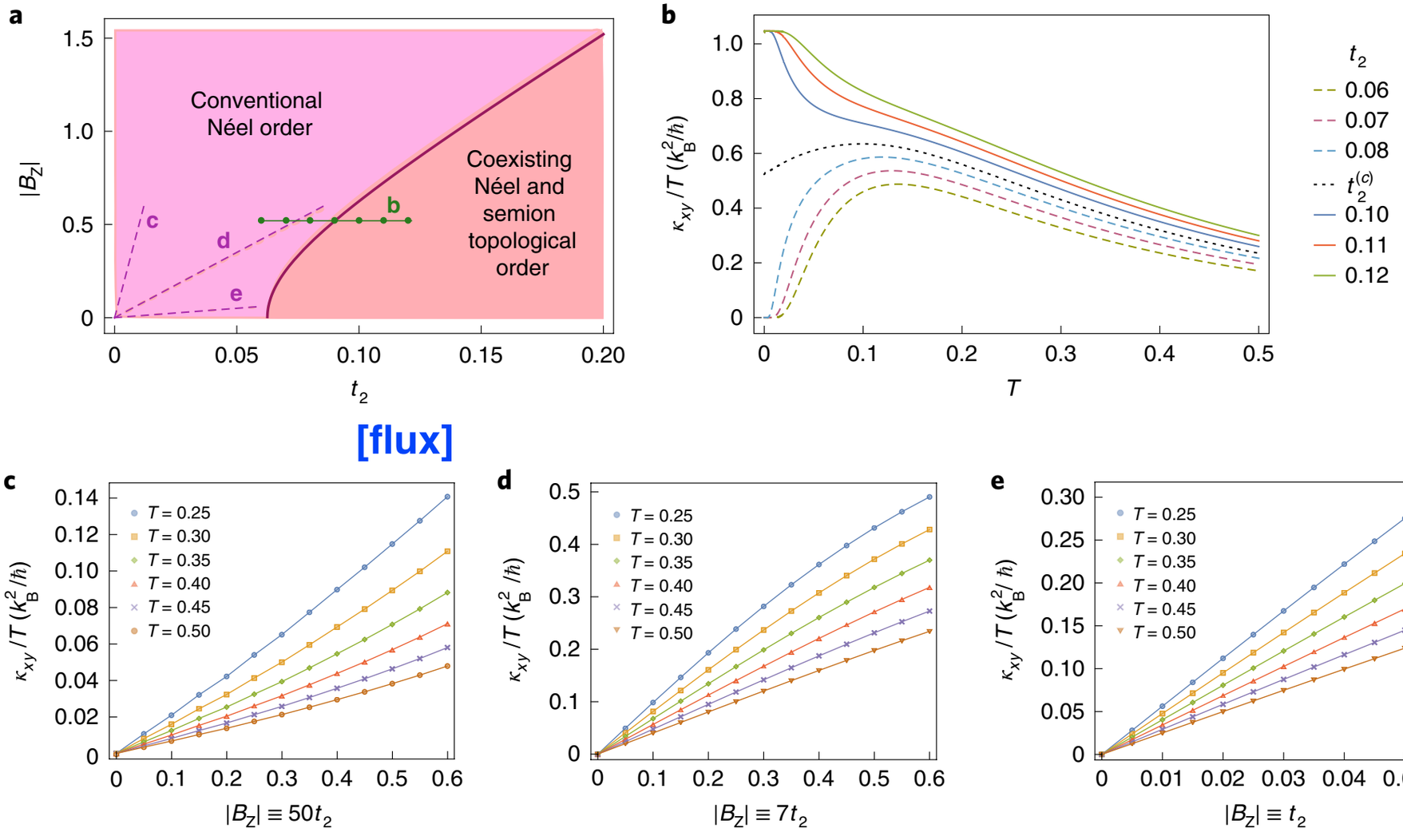

[flux]

Fig. 3 | Phase diagram and thermal Hall conductivity of spinon mean-field theory. a, The two different phases of H_f in equation (3) are shown as a function of it_2 (see Fig. 2a) and $|\mathbf{B}_Z|$. Here, we take $\mathbf{N} = 0.5\hat{z}$ and measure all energies in units of t_1. As discussed in the main text, it_2 is induced by the orbital coupling of the magnetic field. Both t_2 and $|\mathbf{B}_Z|$ are linear functions of the applied magnetic field, and the dashed purple lines show three possible trajectories for which we plot the field dependence of κ_{xy} in **c**–**e** for different T. **b**, Temperature dependence of the mean-field κ_{xy} as t_2 is tuned across the phase boundary; the corresponding discrete values of $|\mathbf{B}_Z|$ and t_2 are indicated by green dots in **a**. The quantized value of the ordinate in the topological phase is $\pi/3$, and the bifurcation point as T approaches 0 is at $\pi/6$. Both values are corrected by gauge fluctuations (the exact quantized value in the topological phase is $\pi/6$). **c**–**e**, Field dependence of κ_{xy} for different T for the trajectories noted in **a** when $|\mathbf{B}_Z| \equiv 50t_2$ (**c**), $7t_2$ (**d**) and t_2 (**e**).

XG Wen&YS Wu , W Chen, MPA Fisher, topological transition

The coupling to scalar spin chirality can come from DM interaction or from higher order perturbation of Hubbard model. The former is tied to the direction of DMI and is probably not a uniform coupling, the later is uniform.

Quote from **Consideration of Thermal Hall Effect in Undoped Cuprates**

Jung Hoon Han,[1,*] Jin-Hong Park,[1] and Patrick A. Lee[2,†]

the very small magnitude. One can make an estimate of J_χ using the t/U expansion by Motrunich [48], to find $J_\chi = -48\pi(t_2 t^2/U^2)(\phi/\phi_0)$ where $\phi_0 = hc/e = 2.07 \times 10^{-15}$Wb is the flux quantum, and $\phi = BA_0$ is the magnetic flux through a triangular plaquete of area $A_0 \approx (3.8\mathring{A})^2/2$ for the cuprate. At $B = 10$T we find $\phi/\phi_0 \approx 3.5 \times 10^{-4}$. Further using commonly accepted values of $t_2 = -0.3t$, $U = 8t$ and $J = 4t^2/U$, we find $J_\chi \approx 5.6 \times 10^{-4} J$ at $B = 10$T. The use of a smaller effective U may increase this number a bit, but in any case a very small number is expected for J_χ, due to the small ratio ϕ/ϕ_0. As we emphasized in this paper, the

Pyrochlore spin ice U(1) QSL

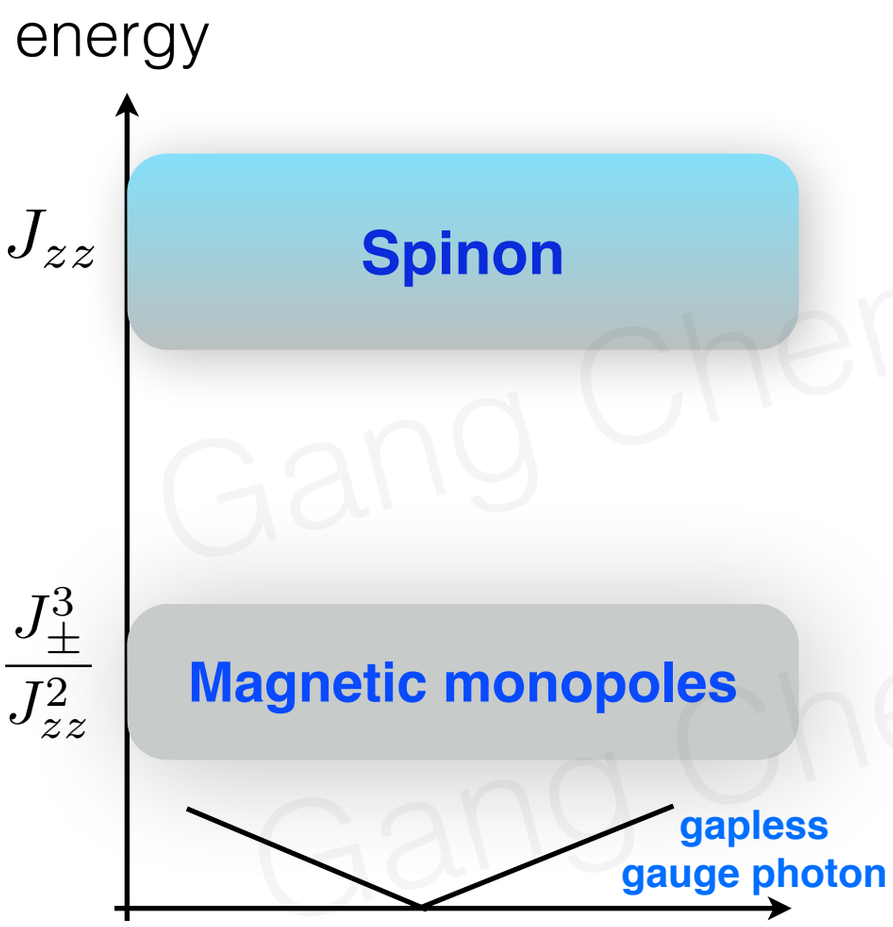

For **non-Kramers doublets** such as Pr ion in $Pr_2Zr_2O_7$ and Tb ion in $Tb_2Ti_2O_7$

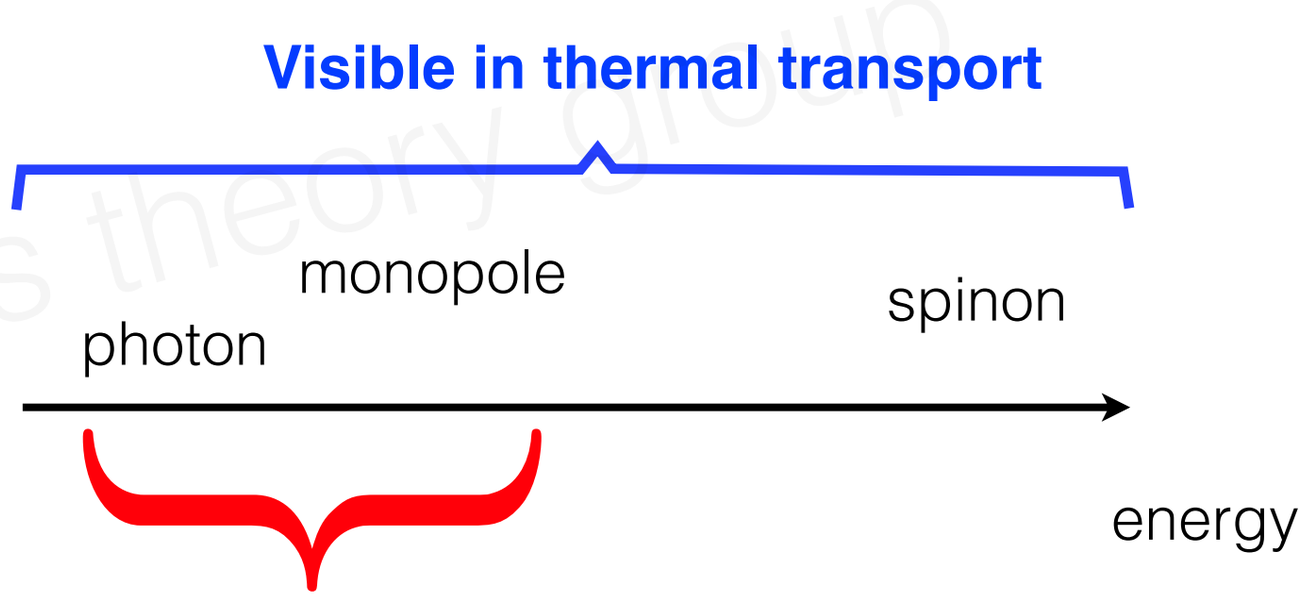

Effect of the external magnetic field

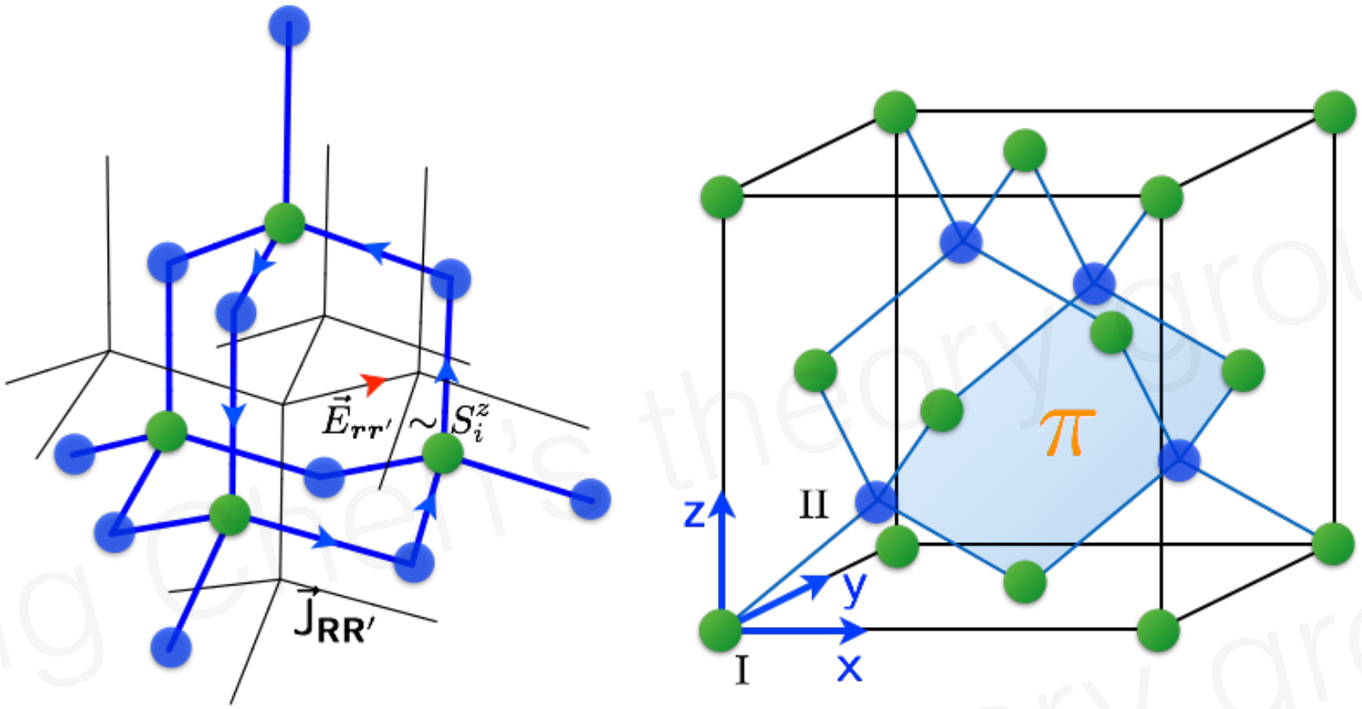

(a) (b)

$$H_{Zeeman} = \vec{B} \cdot \sum_i S_i^z \hat{z}_i$$

The weak magnetic field polarizes Sz slightly, and thus modifies the background electric field distribution. This further modulates monopole band structure, creating "**Hofstadter**" monopole band, which may be detectable in inelastic neutron.

Electromagnetic duality

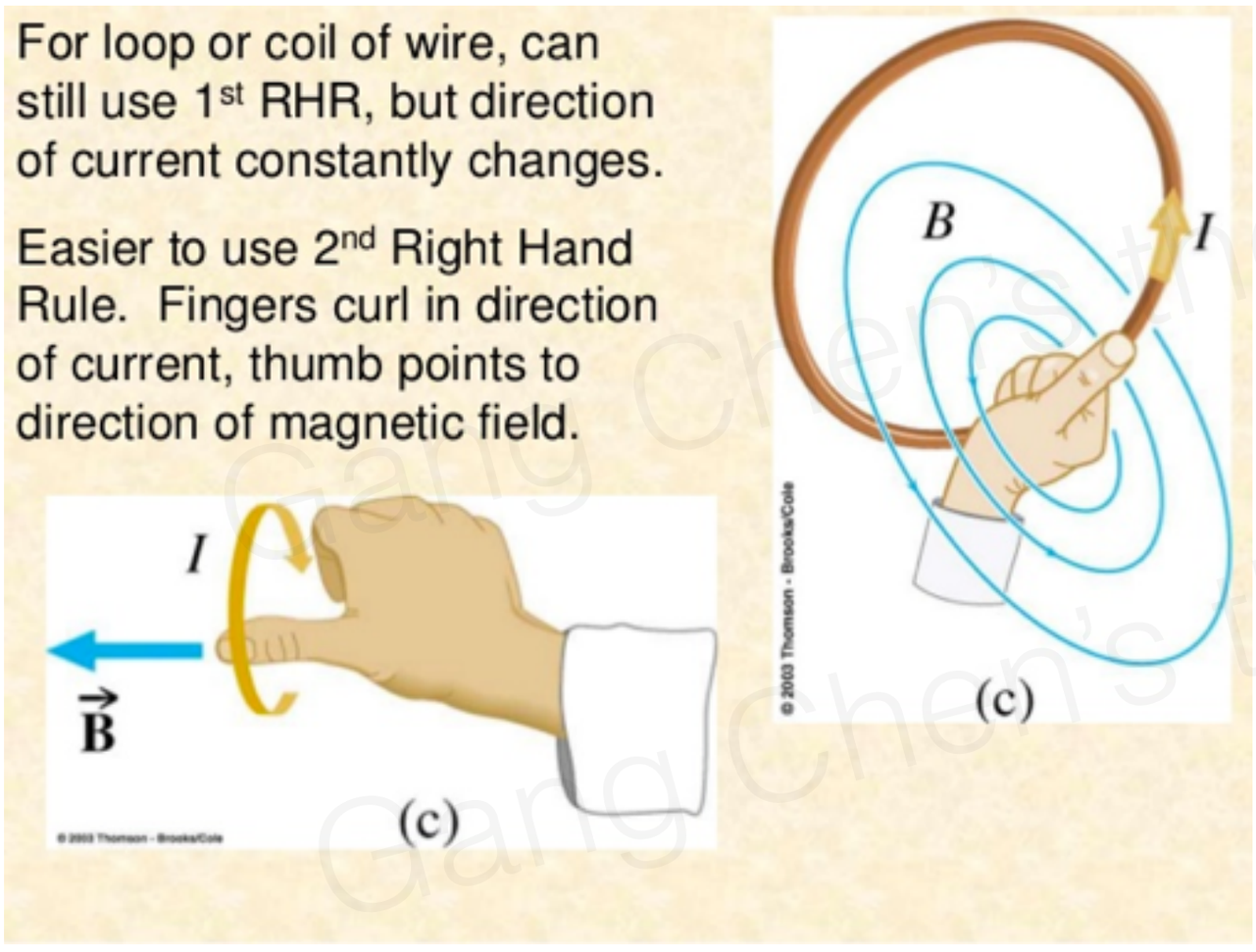

Duality

Electric loop current -> Magnetic field
Magnetic loop current -> Electric field

$S_z \sim E$ (emergent electric field)

G Chen, PRB 96, 195127 (2017)
G Chen, PRB 96, 085136 (2017)

Motrunich & Senthil, 2004,
Bergman, Fiete, Balents, 2006

Xiao-Tian Zhang

Topological thermal Hall effect of "magnetic monopoles" in pyrochlore U(1) spin liquid

Xiao-Tian Zhang[1,4], Yong Hao Gao[2,4], Chunxiao Liu[3], and Gang Chen[4*]
International Center for Quantum Materials, Peking University, Beijing, 100871, China

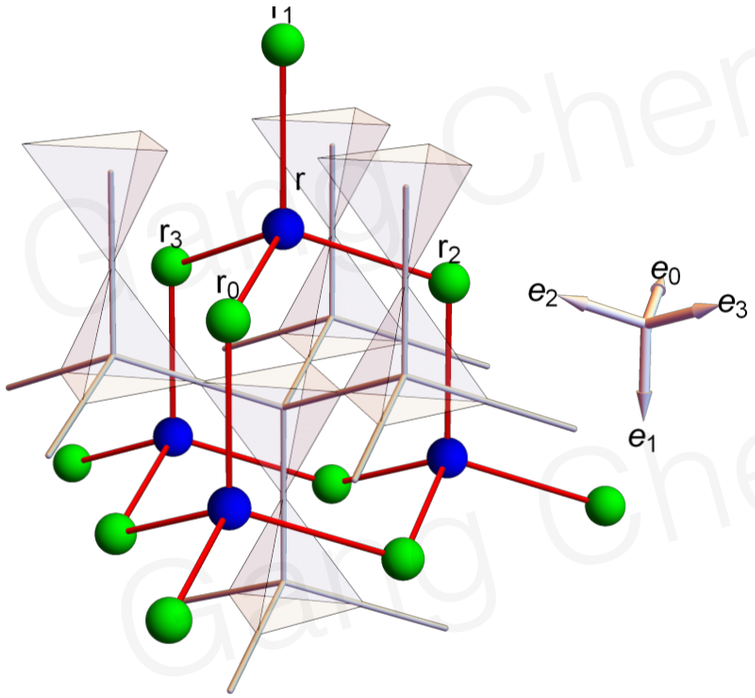

arXiv 1904.08865
PR Research 2020

netic monopoles" and creates a TTHE in the system. The dual Hamiltonian for the "magnetic monopoles", that captures this effect, is given as

$$\begin{aligned}\mathcal{H}_{\text{dual}} =& -t\sum_{\text{rr}'}\Phi_{\text{r}}^{\dagger}\Phi_{\text{r}'}e^{-i2\pi a_{\text{rr}'}} - \mu\sum_{\text{r}}\Phi_{\text{r}}^{\dagger}\Phi_{\text{r}} \\ &+\sum_{rr'}\frac{U}{2}(\text{curl}\ a-\bar{E}_{rr'})^2 - K\sum_{\text{rr}'}\cos B_{\text{rr}'}\end{aligned} \tag{1}$$

$$\begin{aligned}\mathcal{H}_{\text{Zeeman}} =& -g\mu_B H_0\sum_i(\hat{n}\cdot\hat{z}_i)\tau_i^z \\ \simeq& -g\mu_B H_0\sum_i(\hat{n}\cdot\hat{z}_i)(\text{curl}\ a_{rr'}-\bar{E}_{rr'}),\end{aligned}$$

Experiments by P Ong's group on Tb2Ti2O7, Science

Large thermal Hall effect in spin-1/2 Kagome magnets

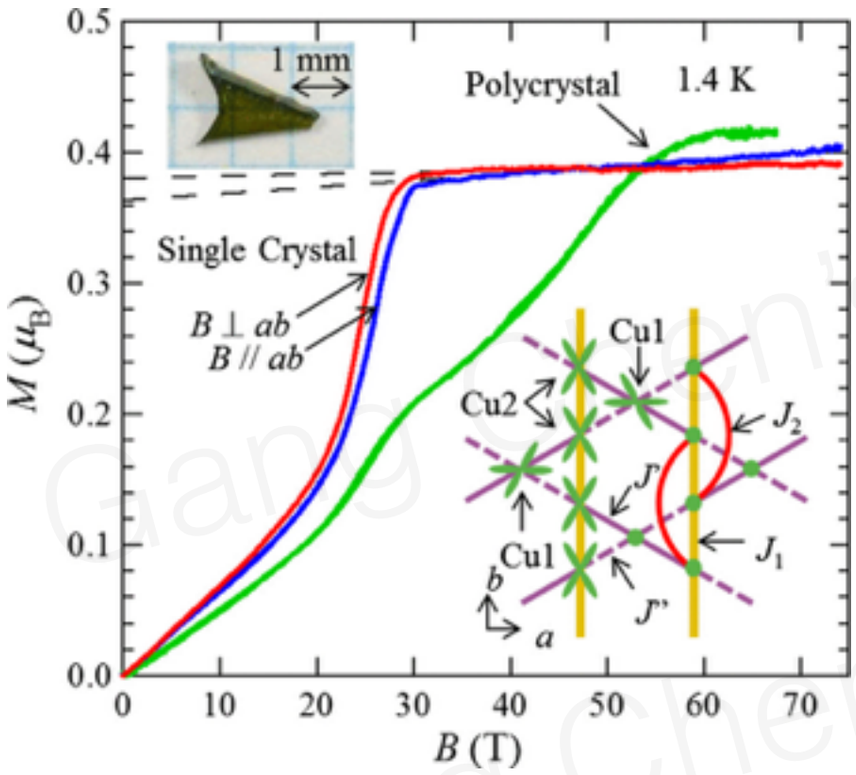

Z Hiroi's group

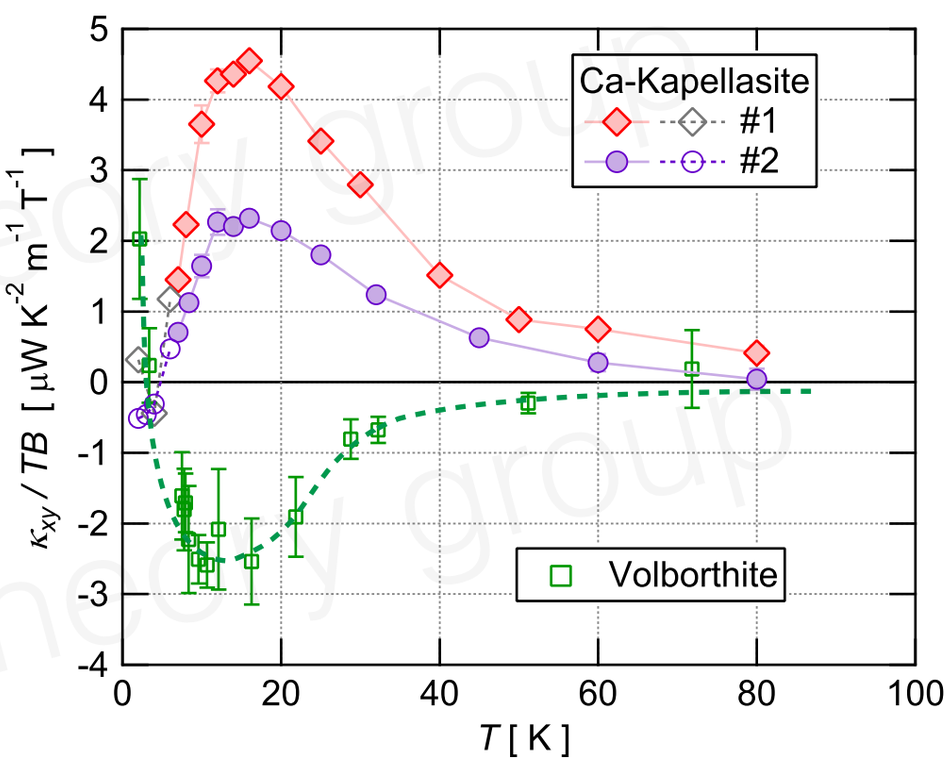

Minoru Yamashita's group

1. Why it is finite? All neutral excitations.
2. Non-monotonic.
3. Opposite signs in two materials.

Our observation: induced internal gauge flux and emergent Lorentz force

Yong Hao Gao

arxiv 1901

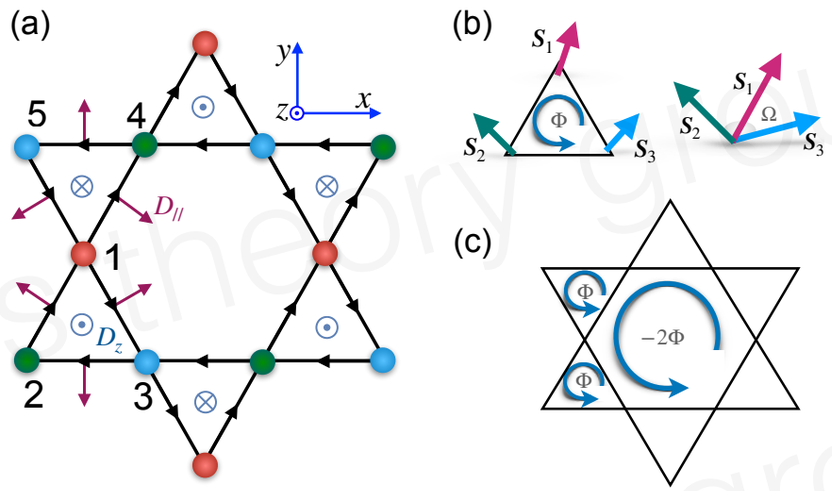

$$H = \sum_{i,j} J_{ij} \boldsymbol{S_i} \cdot \boldsymbol{S_j} + \sum_{i,j} \boldsymbol{D}_{ij} \cdot \boldsymbol{S_i} \times \boldsymbol{S_j} - \sum_i B S_i^z,$$

$$\langle \boldsymbol{S}_i \times \boldsymbol{S}_j \cdot \boldsymbol{S}_k \rangle \sim \langle \boldsymbol{S}_i \times \boldsymbol{S}_j \rangle \cdot \langle \boldsymbol{S}_k \rangle \neq 0$$

The combination of Zeeman coupling and DMI generates an internal U(1) gauge flux distribution.

This provides a way to **control** emergent D.O.F. with external probes.

Topological thermal Hall effect

Yong Hao Gao

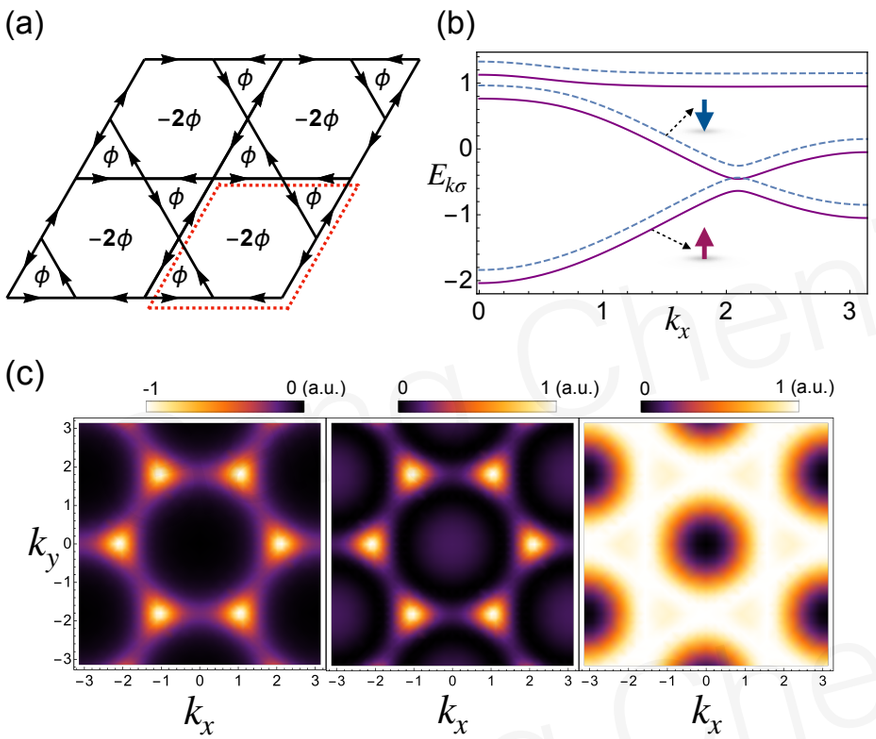

Spinon bands and
Berry curvatures

$$H_{\mathrm{MF}}[\phi] = -t\sum_{\langle ij\rangle}[e^{-i\phi/3}f^{\dagger}_{i\sigma}f_{j\sigma} + h.c.] - \mu\sum_{i} f^{\dagger}_{i\sigma}f_{i\sigma}$$

$$-B\sum_{i,\alpha\beta} f^{\dagger}_{i\alpha}\frac{\sigma^{z}_{\alpha\beta}}{2}f_{i\beta},$$

$$\kappa_{xy} = -\frac{1}{T}\int d\epsilon(\epsilon-\mu)^2\frac{\partial f(\epsilon,\mu,T)}{\partial\epsilon}\sigma_{xy}(\epsilon).$$

$$\sigma_{xy}(\epsilon) = -\sum\nolimits_{\boldsymbol{k},\sigma,\xi_{n,\boldsymbol{k}}<\epsilon}\Omega_{n,\boldsymbol{k},\sigma}$$

Summary

1. point out the physical origin of emergent Lorentz force on spinons and obtain the resulting topological thermal Hall effects.

2. establish the connection between microscopic interactions and emergent D.O.F. and thus provide a scheme to control the emergent D.O.F.

3. Thermal transports in Mott insulators are not well understood. Thermal Hall reflects the internal structure of the excitations.